



Surface hydrogen bonds assisted meso-porous WO_3 photocatalysts for high selective oxidation of benzylalcohol to benzylaldehyde



Yang Su^{a,b}, Zhongkang Han^{b,c}, Ling Zhang^{a,*}, Wenzhong Wang^{a,*}, Manyi Duan^c, Xiaoman Li^{a,b}, Yali Zheng^{a,b}, Yanggang Wang^d, Xiaoling Lei^c

^a State Key Laboratory of High Performance Ceramics and Superfine Microstructure, Shanghai Institute of Ceramics, Chinese Academy of Sciences, 1295 Dingxi Road, Shanghai 200050, PR China

^b University of Chinese Academy of Sciences, Beijing 100049, PR China

^c Division of Interfacial Water and Key Laboratory of Interfacial Physics and Technology, Shanghai Institute of Applied Physics, Chinese Academy of Sciences, 2019 JiaLuo Road, Shanghai 200050, PR China

^d Department of Chemistry, Tsinghua University, Beijing 100084, PR China

ARTICLE INFO

Article history:

Received 20 March 2017

Received in revised form 22 May 2017

Accepted 25 May 2017

Available online 26 May 2017

Keywords:

Selective oxidation
Meso-porous WO_3
Surface fluorination
 H_2O_2
Photocatalytic

ABSTRACT

Selective photo-oxidation of alcohols displays high potential in solar energy conversion and reducing environmental pollution, yet its selectivity and conversion in aqueous phase is still far from expectation. Here we report a fluorinated meso-porous WO_3 photocatalyst (Fm- WO_3) exhibits significant selectivity (~99%) and conversion (~57%) in transforming benzylalcohol to benzylaldehyde in the aqueous solution under the simulated sunlight irradiation. This high reactivity is attributed to the synergistic effect between meso-porous nanostructure and surface fluorination, where meso-porous structure supplies active sites to promote the multi-electron reduction of O_2 and the surface fluorination assists the transmission of photogenerated holes. First-principles calculations further suggest that surface fluorination brings in an unoccupied impurity state in the band structure of WO_3 , which exhibits a strong correlation with the hydroxyl group of benzylalcohol and thus bridges the interaction between surfaces and alcohols. Meanwhile, the fluorination promotes the generation of $\cdot\text{OH}$ by holes which can be considered as another way to oxidize benzylalcohol. Finally, a generalized reaction mechanism for selective photo-oxidation has been proposed.

© 2017 Elsevier B.V. All rights reserved.

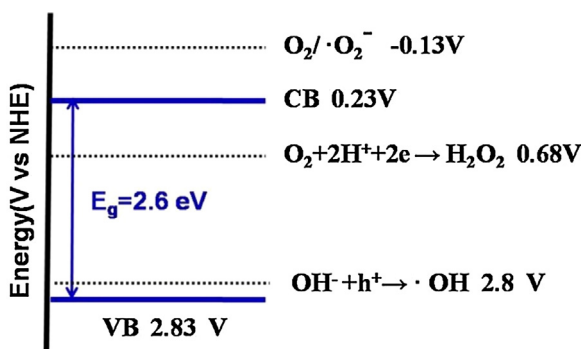
1. Introduction

Selective oxidation of aromatic alcohols [1–3] to corresponding aldehydes is one of the most desirable chemical transformations as the obtained products are important precursors and intermediates for many drugs, vitamins and fragrances [4–7]. Conventional methods including metal-catalyzed aerobic processes [8–10], involved a series problems such as expensive metal catalyst and a large amount of wastes produced in the proceeding [3,11–13]. The development of oxidation processes efficiently utilizing sunlight as an energy source and water as the by product should contribute to the realization of a sustainable society. Photo-catalytic oxidation [14–16] could be a promising chemical oxidation technology for its energy-saving, environmental friendliness and cost-efficiency [17–19].

Tungsten oxide-based compounds have been developed as potential photocatalyst for selective oxidation reaction [18,20,21]. First, the WO_3 exhibited strong Lewis acidity due to the large number of acid sites [22] thus possessed a higher ability to chemisorb and deprotonate alcohol. Second, the photo-generated holes of WO_3 preferentially generate $\cdot\text{OH}$ radicals ($\text{OH}^- + \text{h}^+ = \cdot\text{OH}$ $E^\circ(\text{OH}^-/\cdot\text{OH}) = +2.8\text{ V}$ [23]) rather than directly oxidize chemisorbed species [24]. The indirect oxidation process of hole-generated $\cdot\text{OH}$ exhibited suitable oxidation capacity that can suppress the holes peroxidation process (In the direct hole oxidation process, the oxidation potential of benzaldehyde is about 2.50 V vs. NHE [25]). Last but not least, the electron on the conduction band of the WO_3 layer is not consumed by one-electron reduction of O_2 because the reduction potential ($\text{O}_2 + \text{e} \rightarrow \cdot\text{O}_2^-$, -0.13 V vs. NHE) [25] is more negative than the conduction band potential of WO_3 (Scheme 1). Shiraishi et al. reported that multi-electron reduction of O_2 to the H_2O_2 would be the main path to consume the electrons on the conduction band, because the reduction potentials ($\text{O}_2 + 2\text{H}^+ + 2\text{e} \rightarrow \text{H}_2\text{O}_2$, $+0.68\text{ V}$ vs. NHE) are more positive than the conduction band potential of WO_3 [26]. The

* Corresponding authors.

E-mail address: wzwang@mail.sic.ac.cn (W. Wang).



Scheme 1. The estimated band positions of meso-porous WO_3 .

H_2O_2 then generated hydroxyl radicals ($\cdot\text{OH}$) under illumination which react with alcohols much more efficiently, further increasing conversion for aldehyde. Based on the above principles, recently, Otsubo et al. reported that PdO_x/WO_3 photocatalyst exhibit higher selectivity in comparison to other photocatalysts, such as Pt/WO_3 , Pd/TiO_2 , and Pt/TiO_2 , in the partial oxidation of alcohols to the corresponding aldehydes [24] (e.g. with ~63.1% selectivity for benzyl aldehyde production with ca. 30.6% conversion of benzylalcohol, under the irradiation of a 300 W Xenon lamp with the wavelength range of 300–500 nm for 3 h).

Surface modification of semiconductors can have a remarkable influence on its catalytic performance. Vaiano et al. reported the photocatalytic H_2 production from degradation of glucose by using fluorinated and platinized TiO_2 [27]. The fluorinated surface adsorbed glucose molecules through the H-bond that accelerated the de-prontoned process and degradation. Chen et al. investigated that when TiO_2 surface is covered by F-atoms, which role as H-bonding acceptor, it can enable the holes transferred to the adsorbed molecules favorably. Through the proton-coupled electron transfer process, it facilitates kinetically the cleavage of O–H bonds during water oxidation [28]. Apart from the H-bond effectiveness, fluorination also plays an important role in the separation of carriers. Zhao et al. [29] have proved that the specific-adsorbed anions such as F^- which derived surface negative charges and draw holes to the TiO_2 surface by the electro-static force then enhanced the oxidation of the surface adsorbed species.

Inspired by the above concepts, here, we prepared fluorinated meso-porous WO_3 nanostructure (Fm- WO_3) to replace the expensive Pd metal through a controllable hard template method and a simple fluorination process. As a return for this design, superior selectivity (>99.0%) and conversion (>57.0%) of oxidation of benzylalcohol to benzaldehyde are achieved within expectation. This enhancement originates primarily from (1) proper adsorption mode of benzylalcohol on the Fm- WO_3 surface by formation of surface H-F hydrogen bond; the $\cdot\text{OH}$ from the oxidation of hydroxyl with suitable oxidation ability tended to react with benzylalcohol molecules and suppressing peroxidation. (2) The large surface area resulted from the meso-porous structure supplies more active site for absorbing O_2 molecules to promote efficient multi-electron reduction of O_2 to H_2O_2 which enhanced the oxidation capacity. The synergistic effect between surface fluorination of Fm- WO_3 and meso-porous nanostructure enhances the activity of photocatalytic selective oxidation of benzylalcohol.

2. Experimental

2.1. Preparation of meso-porous WO_3

The meso-porous WO_3 samples were synthesized by a replicating method using meso-porous silica with cubic Ia 3d symmetry (des-

ignated as KIT-6) as a hard template [30]. The meso-porous silica (KIT-6) template was synthesized according to the publiNHEd procedure using triblock copolymer Pluronic P123 (EO20PO70EO20) as a soft template [31]. Meso-porous WO_3 was prepared as following: 2.4 g of phosphotungstic acid was dissolved in 10 mL of ethanol, and this solution was incorporated into 0.8 g of as-prepared KIT-6 by an incipient wetness impregnation technique [32]. The sample was dried and then calcined at 550 °C for 3 h to decompose the precursors, and then further to obtain WO_3 inside the hosting silica. The silica template was removed with 2 M HF solution under the stirring for 6 h. This template-free WO_3 was collected by centrifugation, washed with dilute NaOH to remove adsorbed F during the elimination of template [33] and enough distilled water dried at 60° for 6 h and named as m- WO_3 .

For the further surface fluorination, the pretreated WO_3 (10 g/L) was dispersed in aqueous solutions containing 0.005 M NaF (0.005 M), and the pH was adjusted to 3.5 using HClO_4 . After being stirred overnight at room temperature, the samples were centrifuged, dried. The sample was denoted as Fm- WO_3 .

C-Dots were synthesized by a typical hydrothermal synthesis and treatment [34]. Typically, 0.576 g citric acid was dissolved in 15 mL distilled water to form a transparent solution. The solution was transferred into a stainless steel autoclave and heated at 200 °C for 10 h. After cooled down to room temperature, the product was centrifuged, filtered and washed. The resulting aqueous solution was freeze-dried to obtain the N-doped C-Dots. Then the C-Dots were prepared into a 2 mg/L solution.

2.2. Characterization

The powder X-ray diffraction (XRD) patterns of the synthesized samples were recorded on a D/MAX 2250 diffractometer (Rigaku, Japan) using monochromatized $\text{Cu K}\alpha$ ($\lambda = 0.15418 \text{ nm}$) radiation under 40 kV and 100 mA with the 2θ ranging from 20° to 70°. The diffuse reflectance spectra (DRS) of the samples were obtained on a Hitachi U-3010UV-vis spectrophotometer using BaSO_4 as the reference. The N_2 sorption measurements were performed using a Micromeritics Tristar 3000 porosimeter at 77 K, and the specific surface area and the pore size distribution were calculated using the Brunauer–Emmett–Teller (BET) and Barrett–Joyner–Halenda (BJH) methods, respectively. The microstructures and morphologies of the samples were analyzed by Transmission Electron Microscopy (TEM, FEI Tecnai G2 F30). The photoluminescence spectra (PL) data was recorded on a fluorescence spectrophotometer of Hitachi F-4600 and Shimadzu RF-5301 PC with a 980 nm laser as the excitation source at room temperature. The powder was pressed into plates and the Fourier Transform Infrared (FTIR) spectra were carried out on a FTIR spectrometer (FTIR-7600, Lambda Scientific, Australia).

Subsequently, hydrogen peroxide (H_2O_2) was measured using a (*p*-hydroxyphenyl) acetic acid (POHPAA) analysis method. Typically, a certain volume of fluorescence reagent (potassium hydrogen phthalate: 8.2 g/L, *p*-hydroxyphenylacetic acid: 270 mg/L, and type II horseradish peroxidase: 30 mg/L) was pre-added into the reaction system. 1.0 mL of sample was then withdrawn at an interval time of 2 h and then mixed with 1.0 mL of 1.0 mol/L NaOH for 10 min for measuring the intensity of the fluorescence emission at 409 nm excited at 315 nm [35].

2.3. Electrochemical measurement

Electrochemical measurements were performed on a CHI660D electrochemical workstation (Shanghai Chenhua, China) using a standard three-electrode cell including a working electrode, the counter electrode platinum wire and a reference electrode saturated calomel electrode (SCE). The working electrodes were

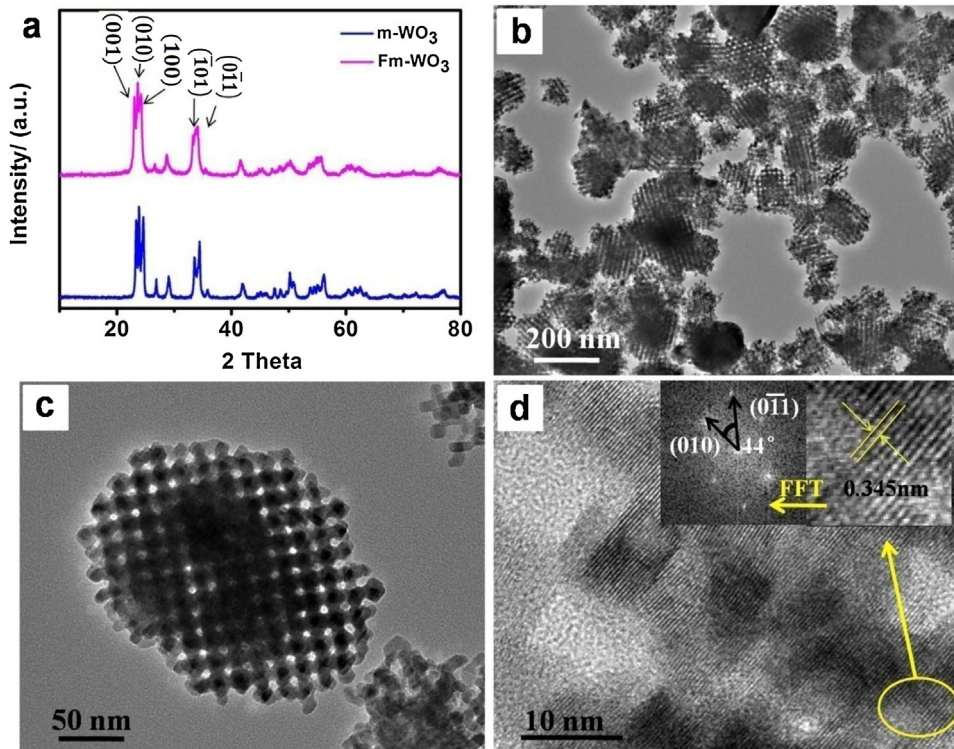


Fig. 1. (a) XRD patterns of m-WO₃ and Fm-WO₃. TEM images of the (b) meso-porous structure of m-WO₃, (c) single particle of m-WO₃, (d) HRTEM of crystal lattice fringes (FFT is the Fast Fourier Transformation).

prepared by dip-coating: 5 mg photocatalyst was suspended in 10 mL ethanol solution and ultrasonicated for 15 min to form slurry. 0.1 mL slurry was dipped onto the fluorine-tin oxide (FTO) glass electrode about 1.5 cm × 2.5 cm square. The film was dried under ambient conditions for 12 h. Here, the electrolyte solution was 0.2 M KCl contained 20% phosphate buffer solution to stabilize the pH of the system [36]. After the electrolyte solution was purged by nitrogen, the measurements of impedance potential method was performed under 100 Hz to get the Mott-Schottky plots. The Zeta potential experiments were performed on Zeta Potential Analyzer (Zetaplus, Brookhaven, USA). In order to avoid the effect of ion concentrations, we sustain the electroconductibility 300 μ S approximately and use NaOH and HCl to adjust the pH(3–9).

2.4. DFT calculations

Calculations were carried out using spin-polarized DFT with generalized gradient approximation (GGA) of Perdew-Burke-Ernzerhof (PBE) implemented in VASP code. The Davidson-block iteration scheme with random initialization of the orbital is used, considering its robustness for most extensive tests. The valence electronic states were expanded in the basis of plane waves with the core-valence interaction represented using the projector augmented wave (PAW) approach and a cutoff of 400 eV. A more accurate single point electronic structure calculation was further performed using the HSE06 functional to obtain the density of states of the WO₃ system. A model structure with twelve atomic layers was used to simulate WO₃ (010) surface. The (2*1) supercells with a vacuum layer of 18 Å were used to exclude the influence of periodic image for the adsorption of benzylalcohol. (1 × 2 × 1) k-points sampling were used.

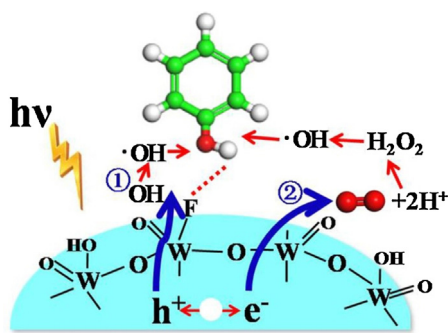
2.5. Photocatalytic oxidation experiments

With a water cooling jacket outside the reactor, the photocatalytic reaction was performed in an open gas circulation under 25 ± 0.5 °C and the light resource was from a 500 W Xe-lamp. Then 0.1 g of photocatalyst was suspended in 50 mL of 0.5 mmol/L benzylalcohol aqueous solution in a Pyrex reaction cell. Subsequently, the solution was magnetically stirred for 1 h in the dark to ensure the establishment of an adsorption–desorption equilibrium between the photocatalyst and benzylalcohol before irradiation. The reaction was continued 4 h for the oxidation. After irradiation, 4 mL suspension were collected, centrifuged and filtered through a 0.22 μ m filter. The clean liquid was used to testing the concentration of benzylalcohol and benzaldehyde. The concentration of reactant and product were measured by a high-performance liquid chromatography (HPLC, injection volume 20 μ L, 0.05% of formic acid aqueous solution/acetonitrile = 30:70, column temperature: 30 °C, flow rate: 0.6 mL/min, detection wavelength: 254 nm). Oxalic acid (C₂H₂O₄) and isopropanol were added to the photocatalytic oxidation system in order to capture the active species holes and •OH in the oxidation process of benzylalcohol [37,38]. The conversion of benzylalcohol and the selectivity for benzaldehyde were defined as follows:

$$\text{Conversion}(\%) = \frac{C_0 - C_{\text{BA}}}{C_0} \times 100 \quad (1)$$

$$\text{Selectivity}(\%) = \frac{C_{\text{BAD}}}{C_0 - C_{\text{BA}}} \times 100 \quad (2)$$

where C₀ is the initial concentration of benzylalcohol and C_{BA} and C_{BAD} are the concentration of the substrate benzylalcohol and the corresponding benzaldehyde, respectively, at a certain time after the photocatalytic reaction.



Scheme 2. Proposed reaction mechanism for the photocatalytic selective oxidation of benzylalcohol over fluorinated meso-porous WO_3 under visible light.

3. Results and discussion

3.1. Characterization of WO_3 photocatalysts

The meso-porous tungsten oxide of monoclinic WO_3 (meso-porous WO_3 is shorten as m- WO_3 here in after.) phase with a high surface area ($45 \text{ m}^2 \text{ g}^{-1}$, the surface area of commercial WO_3 is $5.7 \text{ m}^2 \text{ g}^{-1}$) and average pore size of $6\text{--}9 \text{ nm}$ was prepared by a hard template replicating method (more information shown in Fig. S1). The XRD patterns (Fig. 1a) of m- WO_3 and Fm- WO_3 show that the WO_3 replicas have inherited the meso-porous structure of the KIT6. The meso-porous structure has been maintained after the further fluorinated. All of the diffraction peaks can be indexed to the monoclinic structure of WO_3 (JCPDS Card No. 43-1035). Typical TEM images of the WO_3 are shown in Fig. 1b and c which reveal clearly the meso-porous structure of the as-prepared samples. High-resolution TEM (shown in Fig. 1d) of the prepared m- WO_3 shows clear crystal lattice stripes. The stripes in mesopores can be attributed to WO_3 ($d = 0.345 \text{ nm}$), which is corresponded well with the d-spacing of (010) plane of monoclinic WO_3 .

UV-vis diffuse reflectance spectra (DRS) of meso-porous m- WO_3 and Fm- WO_3 are shown in Fig. 2a. It is found that the absorption edge of m- WO_3 and Fm- WO_3 locate at $\sim 475 \text{ nm}$ and the optical absorptions are ranged from UV to visible light. It is well known that the doping of halogen elements determines a redshift of the absorbance spectrum. Compared with m- WO_3 , further fluorinated treatment has negligible influence on the optical absorption edge of WO_3 . As the fluorination only substituted a portion of surface $-\text{OH}$, the F atoms are not doping into the WO_3 crystal structure. Fluorination treatment has given a noticeable enhanced absorption in the visible light region that means F atoms have been decorated on the surfaces [33,39]. According to the Tauc formula, an indirect band gap of $2.5\text{--}2.6 \text{ eV}$ (inset of Fig. 2a) is estimated for the two samples [40]. To further investigate the electronic characteristics and band position of meso-porous WO_3 , we carried out the electrochemical flat potential measurements and the data was plotted in Mott–Schottky curve (Fig. 2b). Generally, flat-band potential values are determined by using the Mott–Schottky equation [41,42]. The slope of linear $1/C^2$ potential curve was positive, indicating that the as-prepared sample has a n-type semiconductor characteristic. The flat potential is calculated to be 0.230 V versus the normal hydrogen electrode (NHE). Therefore, the top of the valence band is approximately 2.83 eV indicating the holes possess oxidation ability in generating $^{\bullet}\text{OH}$ ($\text{OH}^- + \text{h}^+ = ^{\bullet}\text{OH} \text{ E}^{\circ}(\text{OH}^- / ^{\bullet}\text{OH}) = +2.8 \text{ V}$). As shown in Scheme 1, The e^- on the conduction band of the Fm- WO_3 layer is not consumed by one-electron reduction of O_2 because the reduction potential ($\text{O}_2 + e^- = \text{O}_2^-$, -0.13 V vs. NHE) [25] is more negative than the conduction band potential of WO_3 . The e^- would be consumed by multi-electron reduction of O_2 , which occurs exothermically

because the reduction potentials ($\text{O}_2 + 2\text{H}^+ + 2e^- = \text{H}_2\text{O}_2$, $+0.68 \text{ V}$ vs. NHE; $\text{O}_2 + 4\text{H}^+ + 4e^- = 2\text{H}_2\text{O}$, $+1.23 \text{ V}$ vs. NHE) [20,43,44] are more positive than the conduction band potential of WO_3 . This mechanism is supported by the detail analysis of H_2O_2 formed during reaction in the next section.

The FTIR spectra shown in Fig. 3a demonstrate that the surface structure of samples is significantly changed after the fluorination treatment [33,45]. Most of the surface five-fold-coordinated W atoms are covered by terminal F (as shown in inset of Fig. 3a). For the monoclinic WO_3 crystal, a broad peak appears at $750\text{--}1000 \text{ cm}^{-1}$, which can be assigned to $\text{O}=\text{W}=\text{O}$ stretching vibration ($\nu_{\text{O}=\text{W}=\text{O}}$). A signal can be assignable to the stretching vibration of the surface $-\text{OH}$ groups is observed at 3695 cm^{-1} ($\nu_{-\text{OH}}$), while the signal of deformation vibration of adsorbed water is situated at 1637 cm^{-1} ($\nu_{\text{H}_2\text{O}}$) [46]. In the spectrum of Fm- WO_3 , the signal of both ($\nu_{-\text{OH}}$) and ($\nu_{\text{H}_2\text{O}}$) significantly weakened than that of m- WO_3 . Due to the surface fluorination treatment, the fluorine atom substituted the surface $-\text{OH}$ and occupied the adsorption active sites resulting in the decrease. Fig. 3b shows the zeta potential [47] vs. pH curves of m- WO_3 and Fm- WO_3 . The overall zeta potential of meso-porous m- WO_3 and Fm- WO_3 decreased as the pH increased. Furthermore, it is worth to note that zeta potential of Fm- WO_3 is much more negative than that of m- WO_3 . The fluorinated process could alter the surface energy of the nanoparticles, resulting in different affinity and adsorption of protons on the surface. The more negative Zeta potential means good affinity energy between the surface and proton in the system accelerating the de-protonation process of $-\text{OH}$. The fluorine anions possess stronger electronegativity than oxygen atoms that could better loosen the bond between proton and benzylalcohol then de-protoned.

3.2. Theoretical modeling

To understand the observed high photo-oxidation reactivity, we considered the electronic structure of WO_3 catalyst by employing density functional theory calculations in Fig. 4. The calculated band gap for the pure WO_3 is about 2.5 eV , well consistent with our experimental observation. The surface fluorination is further found not affect the relative position between the valence band and conduction band but introduce an unoccupied impurity state near the Fermi level, which is $\sim 2.2 \text{ eV}$ below the conduction band. This impurity state is expected to strongly interact with the adsorbed species. Furthermore, we consider the adsorption of benzylalcohol on the pure WO_3 and Fm- WO_3 surface (See Fig. 5). It is found that on the pure WO_3 surface the benzylalcohol only physisorbs at the lattice oxygen site via the formation of hydrogen bond with adsorption energy of -0.29 eV . On Fm- WO_3 surface, the benzylalcohol molecule prefers to adsorb on the fluorine site and the adsorption energy is increased to -1.41 eV , suggesting the formation of a strong H-F hydrogen bonds. This is confirmed by the fact that the distance of H-F on Fm- WO_3 surface is only 1.43 \AA while the O–H distance is as large as 1.83 \AA on the pure WO_3 surface. On basis of above discussion, we speculate that it is the impurity state, which originates from the surface fluorination, can effectively correlate with the hydroxyl group of the benzylalcohol molecule via a strong H-F hydrogen bond. This in hence significantly promote de-protonation of benzylalcohol and the formation of hole-generated $^{\bullet}\text{OH}$, thus increase the photo-oxidation conversion. During the whole photo-oxidation process, the fluorine sites on the electro-negative surface work as a bridge that attract electrons from the adsorbate and accelerate the indirect oxidation of the alcohol by the $^{\bullet}\text{OH}$.

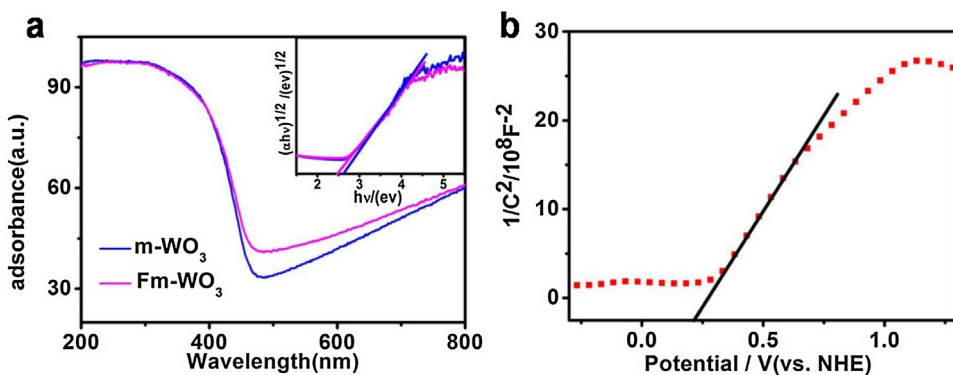


Fig. 2. (a) UV-vis diffuse reflectance spectra of m-WO₃ and Fm-WO₃, (b) Mott-Schottky (MS) plot of m-WO₃.

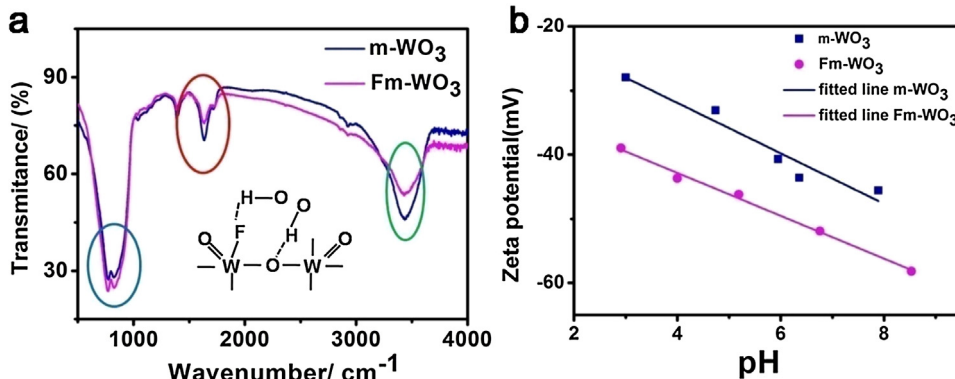


Fig. 3. (a) FT-IR spectra of m-WO₃ and Fm-WO₃, the inset red circle peak at about 1635 cm⁻¹ assigned to H₂O, the inset green circle peak at about 3695 cm⁻¹ assigned to —OH and the inset blue circle peak at about 750–1000 cm⁻¹ assigned to O—W—O stretching vibration (ν —O—W—O). (b) Zeta potential of m-WO₃ and Fm-WO₃. (For interpretation of the references to color in this figure legend, the reader is referred to the web version of this article.)

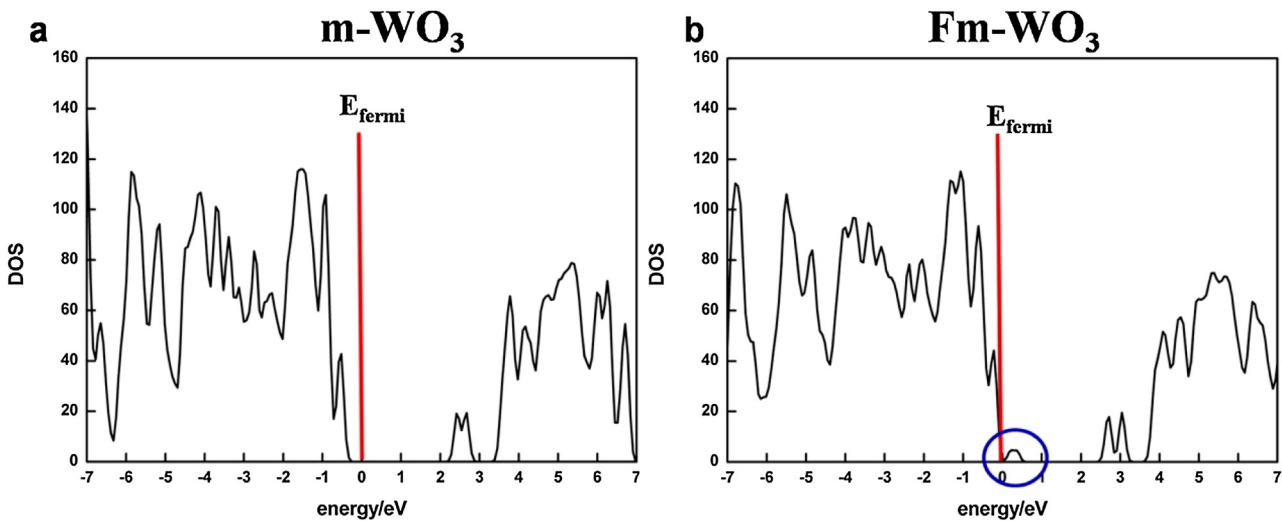


Fig. 4. (a) The density of states of m-WO₃, (b) The density of states of Fm-WO₃. The surface fluorination introduced an unoccupied impurity state near the Fermi level.

3.3. Photocatalytic oxidation of benzylalcohol and active species

The photochemical activities for the selective benzylalcohol oxidation over pristine and fluorinated WO₃ samples were examined by measure the selectivity and conversion. As shown in Table 1, all WO₃ samples exhibit a remarkable selectivity performance (>99%) in benzylalcohol oxidization. The conversion of benzylalcohol to benzylaldehyde rose after the fluorination treatment. The surface fluorinated effect markedly improved the generation of benzalde-

Table 1
The selectivity and conversion rates of WO₃ based photocatalysts.

Catalysts	Selectivity/(\%)	Conversion/(\%)
m-WO ₃	>99	21
Fm-WO ₃	>99	57
Commercial WO ₃	>99	15
F-commercial WO ₃	>99	22

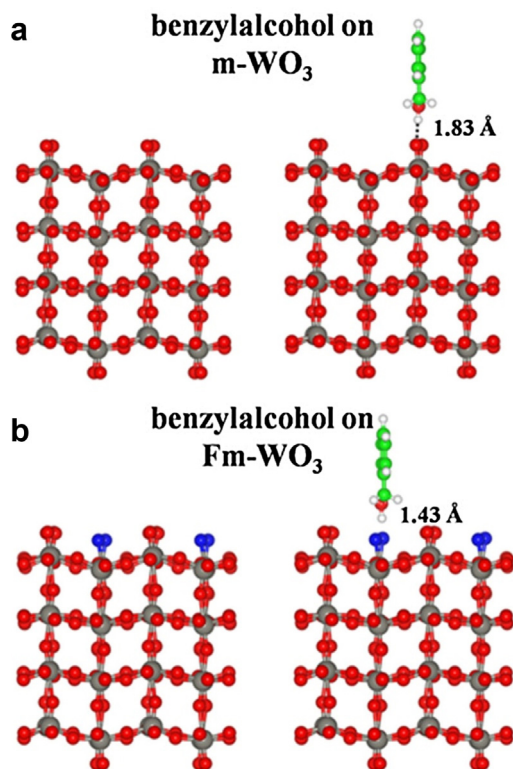


Fig. 5. (a) A benzylalcohol molecule adsorbed onto O site by H-bonding (adsorption on the surface of m-WO₃). (b) a benzylalcohol molecule adsorbed onto F site by H-bonding (adsorption on the surface of Fm-WO₃). The red, gray, blue, green and white balls represented O, W, F, C and H atoms, respectively. (For interpretation of the references to color in this figure legend, the reader is referred to the web version of this article.)

hyde about 57% given a 2-fold increase than that of m-WO₃ and commercial WO₃ powder. The consumptions of benzylalcohol have been plotted in Fig. S2a. Fig. S2b exhibits the kinetics of the oxidation process over the two samples on the basis of the data plotted in Fig. S2a. This results can be described by the first order kinetic model, $\ln(C_0/C) = kt$, where C₀ is the initial concentration and C is the concentration at time t. The rate constant k of m-WO₃ and Fm-WO₃ were calculated to be 0.059 h⁻¹ and 0.206 h⁻¹, respectively, indicating a preferable oxidation performance of Fm-WO₃.

The effect of active species on the oxidation of benzylalcohol was examined by the addition of oxalic acid(OA) as hole scavengers, AgNO₃ as electron scavengers and isoPropyl alcohol (IPA) as •OH scavengers in the presence of Fm-WO₃ [48–50]. As shown in Fig. 6a, an abrupt decrease in the conversion of benzylalcohol was observed by adding either OA to capture photogenerated holes (h⁺), or IPA to capture •OH radicals. These results confirmed that, all the photogenerated holes and the •OH radicals were the influential active species for the present photocatalytic oxidation reaction since photo-generated holes indirectly oxidized benzylalcohol through •OH. When the AgNO₃ solution was added into the reaction system, the conversion of the benzylalcohol increased from 57% to 84%. It suggest that the addition of Ag⁺ significantly increased consumption of the photogenerated electrons (Ag⁺ + e⁻ → Ag, E°(Ag⁺/Ag) = +0.77 V vs NHE), thus increasing the number of active holes on Fm-WO₃ and enhancing the indirect hole oxidation of benzylalcohol on the surface of photocatalyst.

These above results indicated that benzylalcohol was oxidized to produce benzaldehyde on the fluorinated WO₃ photocatalysts by the •OH radical, whereas the reaction rates were greatly influenced by the existence of H₂O₂. Fig. 6b shows the amount of H₂O₂ formed in the as-prepared photocatalyst aqueous solution under

the irradiation of simulated sunlight in the absence of benzylalcohol. The amount of H₂O₂ formed in the aqueous solution increases according the order of commercial-WO₃ < m-WO₃ < Fm-WO₃. The obtained profile of H₂O₂ formation agrees with the oxidation activity of benzylalcohol (Table 1). These data indicate that the e⁻ on the conduction band of WO₃ is consumed by multi-electron reduction of O₂. Meso-porous structure supplies more active sites to adsorb the O₂ molecules for the multi-electron reduction of O₂. Additionally, the surface fluorination treatment promotes the formation of the H-F hydrogen bonds, which can not only enable the holes transfer to the adsorbed molecules thermodynamically, but also facilitate the separation of the photogenerated electron–hole pairs.

However, no accumulated H₂O₂ molecule was detected in the process of oxidation of benzylalcohol(shown in Fig. S4). It suggests that H₂O₂ would react with photo-generated holes (H₂O₂ + 2 h⁺ → O₂ + 2H⁺) [51] or electrons (H₂O₂ + H⁺ + e⁻ → •OH + H₂O, E°(H₂O₂/•OH) = +1.14 V vs NHE; (H₂O₂ + 2H⁺ + 2e⁻ → 2H₂O, E°(H₂O₂/H₂O) = +1.76 V vs NHE) [24] in the photocatalytic reaction system.

3.4. Mechanism for the selective oxidation of benzylalcohol to benzaldehyde on Fm-WO₃

Based on the above results, we propose a mechanism to explain the highly conversion and selective production of benzaldehyde on the Fm-WO₃ photocatalyst (Scheme 2). First, meso-porous WO₃ surface is covered by the H-bonding acceptor F, the first layer benzylalcohol is strongly adsorbed on the surface by a H-bonding adsorption on surface F sites. The high negative charges on the Fm-WO₃ enable the proper affinity of the benzylalcohol and H₂O molecules onto the surface of the photocatalyst in the aqueous media. Photo-generated holes transfer to the surface and generate •OH radials thus holes indirectly oxidize benzylalcohol [52]. Over-oxidation rarely occurred in this system since no over-oxidized product has been detected thus high selectivity was achieved. The hole oxidation may be realized through the indirect oxidation by hydroxyl radicals generated from OH⁻ and water molecules (OH⁻ + h⁺ = •OH E°(OH⁻/•OH) = +2.8 V). Second, photo-generated electrons are consumed for O₂ reduction to H₂O₂ on the meso-porous WO₃ surface. Due to the significantly moderate reactivity of •OH radicals toward benzylaldehyde than toward benzylalcohol, the •OH radicals generated preferentially reacted with the latter, resulting in a steady rate of benzylalcohol generation without CO₂ generation. Meanwhile, the H₂O₂ molecules were likely reduced to •OH acted as an efficient electron scavenger (H₂O₂ + H⁺ + e⁻ → •OH + H₂O, E°(H₂O₂/•OH) = +1.14 V) [24], then contributing to the oxidation of benzylalcohol. By adding carbon nanodots, as a catalyst to decompose of H₂O₂ [35], decreased the concentration of H₂O₂ in the solution and also decreased the conversion of the benzylalcohol (supporting information, Fig. S3). It means the part of •OH radicals came from the deposition of H₂O₂ took part in the oxidation reaction.

4. Conclusion

In summary, we have demonstrated the synergistic effect between meso-porous nanostructure and surface fluorination of Fm-WO₃ to enhance conversion and maintain selectivity of photocatalytic oxidation of benzylalcohol. The surface fluorination promotes the photo-generated holes to oxidize benzylalcohol into benzaldehyde indirectly. Meso-porous structure supplies tremendous active sites to adsorb the O₂ molecules for the multi-electron reduction of O₂ to H₂O₂. Simultaneously, the peroxidation of benzaldehyde to CO₂ is effectively depressed, enabling

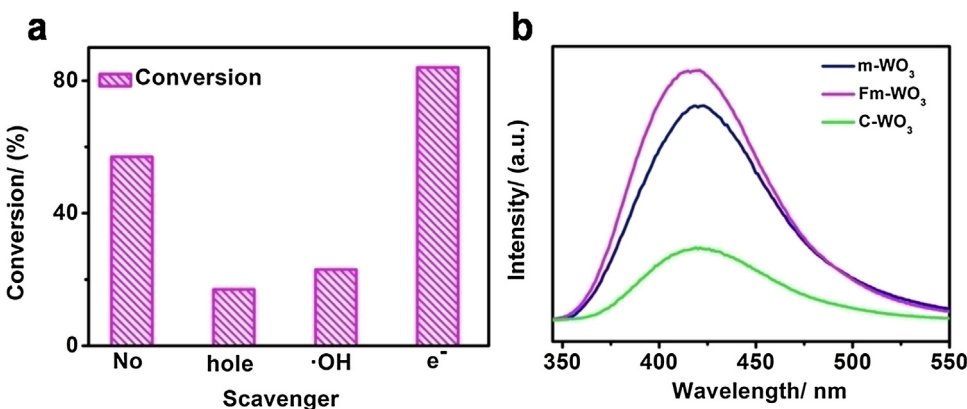


Fig. 6. (a) The conversion of benzylalcohol after different scavenger added in the presence of Fm-WO₃, (b) the photoluminescence (PL) spectra of fluorescence reagent that the peak intensity is proportional to the concentration of H₂O₂ (in the absence of benzylalcohol).

the Fm-WO₃ photocatalyst to generate benzaldehyde from benzylalcohol with very high selectivity.

The H₂O₂ generated in the reaction process were decomposed to ·OH radicals to contribute the oxidation of benzylalcohol. The kinetically favored two-step reaction partway and the enhanced surface reaction rate results in the improved selectivity and conversion of the benzylalcohol oxidation. The discovery of this synergistic effect between decorated surface and mesoporous nanostructure can help design effective photocatalyst systems to replace the noble metal co-catalyst, which is also applicable to other selective conversion applications.

Acknowledgements

We acknowledge the financial support from the 973 Program (2013CB933200) and the National Natural Science Foundation of China (51472260).

Appendix A. Supplementary data

Supplementary data associated with this article can be found, in the online version, at <http://dx.doi.org/10.1016/j.apcatb.2017.05.075>.

References

- J. Long, X. Xie, J. Xu, Q. Gu, L. Chen, X. Wang, *ACS Catal.* 2 (2012) 622–631.
- A.S. Guram, X.H. Bei, H.W. Turner, *Org. Lett.* 5 (2003) 2485–2487.
- Z.R. Tang, Y. Zhang, Y.J. Xu, *ACS Appl. Mater. Interfaces* 4 (2012) 1512–1520.
- M. Caravati, J.D. Grunwaldt, A. Baiker, *Catal. Today* 91–92 (2004) 1–5.
- R. Li, H. Kobayashi, J. Guo, J. Fan, *J. Phys. Chem. C* 115 (2011) 23408–23416.
- Y. Liu, P. Zhang, B. Tian, J. Zhang, *J. ACS Appl. Mater. Interfaces* 7 (2015) 13849–13858.
- R. Marotta, D. Spasiano, I. Di Somma, R. Andreozzi, V. Caprio, *Chem. Eng. J.* 209 (2012) 69–78.
- C. Della Pina, E. Falletta, M. Rossi, *J. Catal.* 260 (2008) 384–386.
- C.Y. Ma, J. Cheng, H.L. Wang, Q. Hu, H. Tian, C. He, Z.P. Hao, *Catal. Today* 158 (2010) 246–251.
- P.J. Miedzialek, Q. He, J.K. Edwards, S.H. Taylor, D.W. Knight, B. Tarbit, C.J. Kiely, G.J. Hutchings, *Catal. Today* 163 (2011) 47–54.
- Y. Yuan, N. Yan, P.J. Dyson, *J. Inorg. Chem.* 50 (2011) 11069–11074.
- Y.M.A. Yamada, T. Arakawa, H. Hocke, Y. Uozumi, *Angew. Chem.* 119 (2007) 718–720.
- X. Lang, X. Chen, J. Zhao, *J. Chem. Soc. Rev.* 43 (2014) 473–486.
- Z. Yang, X. Xu, X. Liang, C. Lei, Y. Wei, P. He, B. Lv, H. Ma, Z. Lei, *Appl. Catal. B-Environ.* 198 (2016) 112–123.
- Y. Hu, Y. Nagai, D. Rahmawaty, C. Wei, M. Anpo, *Catal. Lett.* 124 (2008) 80–84.
- K. Lv, X. Guo, X. Wu, Q. Li, W. Ho, M. Li, H. Ye, D. Du, *Appl. Catal. B-Environ.* 199 (2016) 405–411.
- J.C. Colmenares, W. Ouyang, M. Ojeda, E. Kuna, O. Chernyayeva, D. Lisoviytskiy, S. De, R. Luque, A.M. Balu, *Appl. Catal. B-Environ.* 183 (2016) 107–112.
- G. Lu, X. Li, Z. Qu, Q. Zhao, H. Li, G. Shen, G. Chen, *Chem. Eng. J.* 159 (2010) 242–246.
- F.Z. Su, S.C. Mathew, G. Lipner, X.Z. Fu, M. Antonietti, S. Blechert, X.C. Wang, *Am. Chem. Soc.* 132 (2010) 16299–16301.
- R. Abe, H. Takami, N. Murakami, B. Ohtani, *J. Am. Chem. Soc.* 130 (2008) 7780–7781.
- X.L. Yang, R.H. Gao, W.L. Dai, K.N. Fan, *J. Phys. Chem. C* 112 (2008) 3819–3826.
- Y. Peng, W. Si, X. Li, J. Chen, J. Li, J. Crittenden, J. Hao, *J. Environ. Sci. Technol.* 50 (2016) 9576–9582.
- I.K. Konstantinou, T.A. Albanis, *Appl. Catal. B-Environ.* 49 (2004) 1–14.
- O. Tomita, T. Otsubo, M. Higashi, B. Ohtani, R. Abe, *ACS Catal.* 6 (2016) 1134–1144.
- X. Xiao, J. Jiang, L. Zhang, *Appl. Catal. B-Environ.* 142 (2013) 487–493.
- D. Tsukamoto, Y. Shiraishi, T. Hirai, *Catal. Sci. Technol.* 3 (2013) 2270.
- G. Iervolino, V. Vaiano, J.J. Murcia, L. Rizzo, G. Ventre, G. Pepe, P. Campiglia, M.C. Hidalgo, J.A. Navío, D. Sannino, *J. Catal.* 339 (2016) 47–56.
- H.N.H. Eng, H. Zhang, W. Song, H. Ji, W. Ma, C. Chen, J. Zhao, *J. Angew. Chem. Int. Ed.* 54 (2015) 5905–5909.
- H.N.H. Eng, Q. Li, W.H. Ma, H.W. Ji, C.C. Chen, J.C. Zhao, *Appl. Catal. B-Environ.* 138–139 (2013) 212–218.
- X.Z. Cui, L.M. Guo, F.M. Cui, Q.J. He, J.L. Shi, *J. Phys. Chem. C* 113 (2009) 4134–4138.
- X.Z. Cui, J.L. Shi, H.R. Chen, L.X. Zhang, L.M. Guo, J.H. Gao, J.B. Li, *J. Phys. Chem. B* 112 (2008) 12024–12031.
- X.Z. Cui, H. Zhang, X.P. Dong, H.R. Chen, L.X. Zhang, L.M. Guo, J.L. Shi, *J. Mater. Chem.* 18 (2008) 3575–3580.
- K. Villa, S. Murcia-López, T. Andreu, J.R. Morante, *Catal. Commun.* 58 (2015) 200–203.
- Y. Zhang, Y. Wang, X. Feng, F. Zhang, Y. Yang, X. Liu, *Appl. Surf. Sci.* 387 (2016) 1236–1246.
- S. Li, G. Dong, R. Hailili, L. Yang, Y. Li, F. Wang, Y. Zeng, C. Wang, *Appl. Catal. B-Environ.* 190 (2016) 26–35.
- B. Klahr, S. Gimenez, F. Fabregat-Santiago, T. Hamann, J. Bisquert, *J. Am. Chem. Soc.* 134 (2012) 4294–4302.
- S. Chen, Y. Hu, S. Meng, X. Fu, *Appl. Catal. B-Environ.* 150–151 (2014) 564–573.
- M. Xie, X. Dai, S. Meng, X. Fu, S. Chen, *Chem. Eng. J.* 245 (2014) 107–116.
- A. Vijayabalan, K. Selvam, R. Velmurugan, M. Swaminathan, *J. Hazard. Mater.* 172 (2009) 914–921.
- M.A. Butler, *J. Appl. Phys.* 48 (1977) 1914.
- S.K. Maiti, S. Banerjee, A.K. Mukherjee, K.M. Abdul Malik, R. Bhattacharyya, *New J. Chem.* 29 (2005) 554.
- A. Ishikawa, T. Takata, J.N. Kondo, M. Hara, H. Kobayashi, K. Domen, *J. Am. Chem. Soc.* 124 (2002) 13547–13553.
- O. Tomita, B. Ohtani, R. Abe, *Catal. Sci. Technol.* 4 (2014) 3850–3860.
- J. Liu, Y. Liu, N.Y. Liu, Y.Z. Han, X. Zhang, H. Huang, Y. Lifshitz, S.T. Lee, J. Zhong, Z.H. Kang, *Science* 347 (2015) 970–974.
- S.M. Kanan, Z.X. Lu, J.K. Cox, G. Bernhardt, C.P. Tripp, *Langmuir* 18 (2002) 1707–1712.
- M. Teranishi, R. Hoshino, S. Naya, H. Tada, *Angew. Chem. Int. Ed. Engl.* 55 (2016) 12773–12777.
- M. Haruta, *J. New Mater. Electrochem. Syst.* 7 (2004) 163–172.
- K. Zhao, L. Zhang, J. Wang, Q. Li, W. He, J.J. Yin, *J. Am. Chem. Soc.* 135 (2013) 15750–15753.
- J. Yang, X. Wang, Y. Chen, J. Dai, S. Sun, *RSC Adv.* 5 (2015) 9771–9782.
- L. Yuan, Q. Yu, Y. Zhang, Y.-J. Xu, *RSC Adv.* 4 (2014) 15264.
- H. Dotan, K. Sivula, M. Grätzel, A. Rothschild, S.C. Warren, *Energy Environ. Sci.* 4 (2011) 958–964.
- Q. Vanessa, M. Hellström, J. Behler, *J. Phys. Chem. Lett.* 8 (2017) 1476–1483.